January 1, 2009

Nonmodal and Nonlinear Dynamics of a Volatile Liquid Film Flowing over a Locally Heated Surface

N Tiwari
JM Davis

Nonmodal and nonlinear dynamics of a volatile liquid film flowing over a locally heated surface

Naveen Tiwari and Jeffrey M. Davis

Citation: Physics of Fluids (1994-present) **21**, 102101 (2009); doi: 10.1063/1.3241967
View online: http://dx.doi.org/10.1063/1.3241967
View Table of Contents: http://scitation.aip.org/content/aip/journal/pof2/21/10?ver=pdfcov
Published by the AIP Publishing

Nonmodal and nonlinear dynamics of a volatile liquid film flowing over a locally heated surface

Naveen Tiwari and Jeffrey M. Davis[a)]
Department of Chemical Engineering, University of Massachusetts, Amherst, Massachusetts 01003, USA

(Received 7 April 2009; accepted 10 September 2009; published online 1 October 2009)

The stability of a thin, volatile liquid film falling under the influence of gravity over a locally heated, vertical plate is analyzed in the noninertial regime using a model based on long-wave theory. The model is formulated to account for evaporation that is either governed by thermodynamic considerations at the interface in the one-sided limit or limited by the rate of mass transfer of the vapor from the interface. The temperature gradient near the upstream edge of the heater induces a gradient in surface tension that opposes the gravity-driven flow, and a pronounced thermocapillary ridge develops in the streamwise direction. Recent theoretical analyses predict that the ridge becomes unstable above a critical value of the Marangoni parameter, leading to the experimentally observed rivulet structure that is periodic in the direction transverse to the bulk flow. An oscillatory, thermocapillary instability in the streamwise direction above the heater is also predicted for films with sufficiently large heat loss at the free surface due to either evaporation or strong convection in the adjoining gas. This present work extends the recent linear stability analysis of such flows by Tiwari and Davis [Phys. Fluids **21**, 022105 (2009)] to a nonmodal analysis of the governing non-self-adjoint operator and computations of the nonlinear dynamics. The nonmodal analysis identifies the most destabilizing perturbations to the film and their maximum amplification. Computations of the nonlinear dynamics reveal that small perturbations can be sufficient to destabilize a linearly stable film for a narrow band of wave numbers predicted by the nonmodal, linearized analysis. This destabilization is linked to the presence of stable, discrete modes that appear as the Marangoni parameter approaches the critical value at which the film becomes linearly unstable. Furthermore, the thermocapillary instability leads to a new, time-periodic base state. This transition corresponds to a Hopf bifurcation with increasing Marangoni parameter. A linear stability analysis of this time-periodic state reveals further instability to transverse perturbations, with the wave number of the most unstable mode about 50% smaller than for the rivulet instability of the steady base state and exponential growth rate about three times larger. The resulting film behavior is reminiscent of inertial waves on locally heated films, although the wave amplitude is larger in the present case near the heater and decays downstream where the Marangoni stress vanishes. The film's heat transfer coefficient is found to increase significantly upon the transition to the time-periodic flow. © *2009 American Institute of Physics*. [doi:10.1063/1.3241967]

I. INTRODUCTION

Many industrial and technological applications involve thin liquid films flowing over heated surfaces, including coating processes, material processing flows, energy systems with evaporative cooling, thermal management of electronic devices, and separation processes. Because the surface tension of a liquid-gas interface depends on the temperature, a temperature variation along the interface induces a surface-tension gradient, or Marangoni stress.[1] In thin liquid layers, the thermocapillary flow associated with these tangential stresses can make the film unstable to infinitesimal perturbations that grow and ultimately lead to spatiotemporal pattern formation or even film rupture.[2,3] Evaporation can significantly influence the temperature distribution in liquid films, and models have recently been developed to study its effects on the dynamics of locally heated films[4] and the Bénard–Marangoni instability.[5] Detailed theoretical analyses have been used to explore the stability of liquid films on heated, horizontal surfaces[6] and for films flowing down uniformly heated, inclined planes.[7–10] In addition, gravity-driven flow down inclined surfaces with nonuniform heating has been investigated recently.[11–15]

While most of these studies were focused on the interaction of the inertial surface-wave instability with thermocapillary effects, there has also been much recent theoretical work on pattern formation in liquid films flowing over locally heated surfaces,[16–23] in which interesting dynamics occur even in the noninertial limit. These studies were motivated by a series of experiments in which a thin liquid film flows over an inclined plane wall bearing a rectangular heater.[24–27] The temperature gradient at the upstream edge of the heater induces the formation of a two-dimensional bump, or thermocapillary ridge, in the streamwise direction, and the bump height increases with the heat flux from the heater. At a critical value of the heat flux, the film becomes unstable to disturbances with transverse wave numbers in a finite band

[a)]Electronic mail: jmdavis@ecs.umass.edu.

separated from zero,[20] and a periodic array of longitudinal rivulets forms at the downstream edge of the bump.

A linear stability analysis of models based on long-wave theory revealed the existence of both a discrete and a continuous spectrum.[19,21,23] The continuous spectrum consists of eigenfunctions that approach bounded oscillations at the infinities, is described by the dispersion relation of a flat film, and is always stable. The discrete spectrum is unstable beyond a critical Marangoni number for a band of wave numbers in the interval (q_1,q_2) with $q_1>0$, corresponding to a rivulet instability that is consistent with published results from experiment and direct numerical simulation.[20]

Because the spatial nonuniformity of the base state gives rise to non-normal (not self-adjoint) linearized operators that govern the evolution of perturbations, Tiwari *et al.*[21] performed a transient, nonmodal analysis to study the short-time dynamics of perturbations in the limit of negligible heat transfer from the film (vanishing Biot number). The transient amplification of perturbations was found to be essentially negligible for unstable wave numbers because the (unstable) discrete eigenfunction is nearly orthogonal to the (stable) continuous modes. Weak transient amplification was found for stable wave numbers, indicating that nonmodal effects are insignificant for noninertial flows over locally heated surfaces in the limit of vanishing Biot number. Tiwari and Davis[23] subsequently examined the linear stability of a volatile liquid film flowing over a locally heated surface. Evaporation results in significant heat transfer from the film to the surrounding gas (analogous to larger Biot number), and the interfacial temperature depends not only on the substrate temperature but also on the local film thickness, such that spatial variations in the film thickness induce thermocapillary flow. The resulting dynamics and dispersion curves can be significantly more complex than in the vanishing Biot number limit, as evidenced by the presence of an oscillatory, thermocapillary instability[23] in addition to the rivulet instability investigated previously.

It is therefore of interest to extend the model of Tiwari and Davis[23] to study the nonmodal and nonlinear dynamics of these flows. In this present paper, the dynamics and stability of a thin, volatile liquid film falling under the influence of gravity down a locally heated, vertical plate are analyzed in the noninertial regime using a model based on long-wave theory. The evolution equation developed by Tiwari and Davis,[23] which also forms the basis for this work, is briefly summarized in Sec. II. Representative film profiles and dispersion curves from a linear stability analysis, which are used to interpret results in subsequent sections, are presented in Secs. III A and III B, respectively. Results of a nonmodal, transient analysis are presented in Sec. III C. The optimal perturbations, which elucidate the regions of the film most sensitive to disturbances, are presented in Sec. III D. The pseudospectra of the governing linearized operator are shown in Sec. III E. Results from the nonlinear evolution of the perturbed film are presented in Sec. III F, including the nonlinear growth rate of perturbations, perturbation magnitude that destabilizes a linearly stable flow, time-periodic base states that correspond to a Hopf bifurcation of the steady base state (and which are attained through the nonlinear saturation of a thermocapillary instability), and the linear stability of these time-periodic base states to transverse perturbations. Conclusions are presented in Sec. IV.

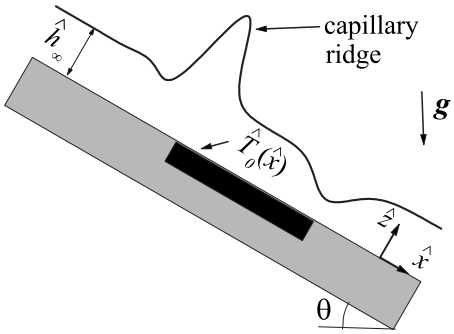

FIG. 1. Schematic diagram of a thin liquid film flowing over a heater. The Marangoni stress at the upstream edge of the heater opposes the gravitational flow, which leads to the formation of a capillary ridge.

II. PROBLEM FORMULATION

Consider a thin liquid film with density ρ, viscosity μ, and thermal diffusivity α_{th} flowing under the influence of gravity over a planar substrate inclined from the horizontal by angle θ. The film flows along the plane in the $\hat{x}$-direction, $\hat{z}$ is directed outwardly normal from the substrate, and $\hat{y}$ is the transverse coordinate in the plane of the substrate. A rectangular heater is embedded in the substrate, as shown schematically in Fig. 1, and generates the temperature profile $\hat{T}(\hat{x},\hat{y},\hat{z})=\hat{T}_0(\hat{x})$ at the solid surface, with $\hat{T}_H=\max(\hat{T}_0)$. Far upstream of the heater, the film has constant thickness $\hat{h}=\hat{h}_\infty$, corresponding to the liquid being supplied at a constant flow rate. The liquid has surface tension γ_0 at the ambient temperature $\hat{T}=\hat{T}_\infty$. A linear variation of surface tension with temperature is assumed, i.e., $\gamma(\hat{T})=\gamma_0-\gamma_T(\hat{T}-\hat{T}_\infty)$, where $\gamma_T>0$ and $\gamma_T\equiv\partial\gamma/\partial\hat{T}$.

Dimensionless quantities are formulated by introducing scaled variables,

$$(z,h)=(\hat{z},\hat{h})/\hat{h}_\infty,\quad (x,y)=(\hat{x},\hat{y})/l_c,$$

$$T=(\hat{T}-\hat{T}_\infty)/\Delta\hat{T},\quad p=\hat{p}/(\gamma_0\,\mathrm{Ca}^{2/3}/\hat{h}_\infty),$$

$$l_c=\hat{h}_\infty(3\,\mathrm{Ca})^{-1/3},\quad \Delta\hat{T}\equiv\hat{T}_H-\hat{T}_\infty, \tag{1}$$

$$U=(\rho g\hat{h}_\infty^2\sin\theta)/(3\mu),\quad G=(3\,\mathrm{Ca})^{1/3}\cot\theta,$$

$$M=3^{1/3}\gamma_T\Delta\hat{T}/(2\gamma_0\,\mathrm{Ca}^{2/3}),\quad J=\hat{J}(\Delta H_{\text{vap}}\hat{h}_\infty/k\Delta\hat{T}),$$

where l_c is the dynamic capillary length, $\mathrm{Ca}=\mu U/\gamma_0$ is the capillary number, U is the characteristic velocity of the falling film, and ΔH_{vap} is the latent heat of vaporization. The Marangoni parameter M characterizes the magnitude of the surface-tension gradient from the nonuniform temperature profile at the heater. The parameter $G\equiv[(\rho g\hat{h}_\infty^2/\gamma_0)\sin\theta]^{1/3}\cot\theta$ can also be expressed in terms of a Bond number $(\mathrm{Bo}=\rho g\hat{h}_\infty^2/\gamma_0)$ based on the film thick-

TABLE I. Definition and physical interpretation of dimensionless groups.

Parameter	Definition	Physical interpretation
Re	$\rho U\hat{h}_\infty/\mu$	Ratio of inertia to viscous forces
Ca	$\mu U/\gamma_0$	Ratio of viscous force to surface-tension force
Pe	$U\hat{h}_\infty/\alpha_{\text{th}}$	Ratio of convective heat transfer in flowing film to conduction across film
M	$3^{1/3}\gamma_T\Delta\hat{T}/(2\gamma_0\,\text{Ca}^{2/3})$	Dimensionless surface-tension gradient
K_{OS}	$k\hat{T}_\infty^{3/2}(2\pi R_g/M_w)^{1/2}/(\alpha\hat{h}_\infty\rho^v\Delta H_{\text{vap}}^2)$	Dimensionless vapor pressure driving force for net mass transfer from free surface
K_{MT}	$kR_g\hat{T}_\infty^2/(k_m\rho^v\hat{h}_\infty M_w\Delta H_{\text{vap}}^2)$	Ratio of heat transfer resistance between free surface and surrounding gas to thermal resistance from conduction across liquid film
Bi	$\hat{h}_\infty k_H/k\equiv K^{-1}$ if $E\to 0$	Biot number
E	$k\Delta\hat{T}/(\rho U\hat{h}_\infty\Delta H_{\text{vap}})$	Ratio of convective time scale to evaporative time scale

ness. The key dimensionless parameters are summarized in Table I.

With the constraints $\text{Ca}^{2/3}\ll 1$, $\text{Re}\,\text{Ca}^{1/3}\ll 1$, and $\text{Pe}\,\text{Ca}^{1/3}\ll 1$, where $\text{Re}=\rho U\hat{h}_\infty/\mu$ is the Reynolds number and $\text{Pe}=U\hat{h}_\infty/\alpha_{\text{th}}$ is the thermal Peclet number, the governing Navier–Stokes, energy, and continuity equations can be reduced to the leading-order evolution equation for the film,[23]

$$\frac{\partial h}{\partial t}+EJ+\nabla\cdot[(\boldsymbol{e}_x+\nabla\nabla^2 h-G\nabla h)h^3-M\nabla T^i h^2]=0, \tag{2}$$

which is similar to evolution equations derived in many other studies of thin liquid films.[1] Here, $E=(k\Delta\hat{T})/(\rho U\hat{h}_\infty\Delta H_{\text{vap}})$ is a dimensionless evaporation number that is a ratio of the convective time scale, $t_c=\hat{h}_\infty/U$, to the evaporative time scale, $t_e=(\rho h_\infty^2\Delta H_{\text{vap}})/(k\Delta\hat{T})$, and k is the thermal conductivity of the liquid. In the remainder of this work, attention is restricted to a vertical substrate, $\theta=\pi/2$, so $G=0$. Vapor recoil[6] is neglected in this analysis.

The interfacial temperature is $T^i=KT_0/(K+h)$, and the (dimensionless) mass flux is $J=T_0/(K+h)$.[23] The parameter K behaves as an inverse Biot number that quantifies the resistance to heat transfer from the free surface to the surrounding gas relative to the thermal resistance from conduction across the liquid film.[28] This parameter can be defined in several ways depending on how heat transfer from the film to the gas is modeled.

In the one-sided evaporation limit,[6,28] the interfacial temperature $\hat{T}^i$ is related to the mass flux using a linearized constitutive equation derived from kinetic theory,[29]

$$\hat{J}=\left(\frac{\varepsilon_E\rho^v\Delta H_{\text{vap}}}{\hat{T}_\infty^{3/2}}\right)\left(\frac{M_w}{2\pi R_g}\right)^{1/2}(\hat{T}^i-\hat{T}_\infty), \tag{3}$$

where M_w is the molecular weight, R_g is the universal gas constant, and ρ^v is the vapor density. The dimensionless, empirical evaporation coefficient ε_E was defined[28,30] as the ratio of the observed to calculated evaporation rate and has been used to correlate a large number of measurements.[31] This coefficient has been shown to be a small parameter $\varepsilon_E<1$, with reported values for water ranging from 0.0002 to 0.3 in many experimental studies at 1 atm and 20–50 °C.[30] Smaller values of ε_E are common for polar liquids or when trace impurities are present at the liquid-gas interface.[30] In this one-sided model, mass transfer (diffusion) of the vapor is assumed to be very fast, corresponding to the limit of large Peclet number in the gas phase.[32] Consequently, the vapor density is spatially uniform, and the evaporation rate is determined only from thermodynamic considerations at the liquid-vapor interface. The parameter K is then defined as $K_{\text{OS}}=[k\hat{T}_\infty^{3/2}(2\pi R_g/M_w)^{1/2}/\varepsilon_E\hat{h}_\infty\rho^v\Delta H_{\text{vap}}^2]$.

In many situations, the rate of mass transfer of the vapor from the interface limits the evaporation rate. For this case, with the gas phase saturated in vapor in the vicinity of the interface,[32] the evaporation rate is equal to the rate at which vapor is transported away from the interface,

$$\hat{J}=k_m(\rho^v|_{\text{int}}-\rho_\infty^v), \tag{4}$$

where k_m is the mass transfer coefficient, $\rho^v|_{\text{int}}$ is the vapor density at the interface, and ρ_∞^v is the vapor density in the bulk gas away from the interface as $\hat{z}\to\infty$. For small differences between $\hat{T}^i$ and $\hat{T}_\infty$ such that $\rho^v(\hat{T})$ can be linearized,[23] $K_{\text{MT}}=kR_g\hat{T}_\infty^2/k_m\rho^v\hat{h}_\infty M_w\Delta H_{\text{vap}}^2$. If $k_m\to\infty$ then thermodynamic effects at the interface must be taken into account as in the one-sided model.

For the case of a nonvolatile liquid, heat transfer from the free surface to the surrounding gas is characterized by a heat transfer coefficient k_H, and the interfacial energy balance is

$$-k\boldsymbol{n}\cdot\nabla\hat{T}=k_H(\hat{T}-\hat{T}_\infty)\quad\text{at}\quad\hat{z}=\hat{h}(\hat{x},\hat{y}). \tag{5}$$

In this limit, $E\to 0$ and $K\equiv\text{Bi}^{-1}$, with $\text{Bi}=\hat{h}_\infty k_H/k$ the Biot number. As a consequence of the different physical mechanisms that govern heat loss from the film, the admissible range of values for K is large.[23]

The boundary conditions for Eq. (2) correspond to a uniform film away from the heater,

$$h \to 1, \quad h_x \to 0 \quad \text{as} \quad x \to -\infty,$$
$$h_x \to 0, \quad h_{xxx} \to 0 \quad \text{as} \quad x \to \infty. \tag{6}$$

Because there is mass loss from evaporation as the film flows over the heater, $h \to c_1$ as $x \to \infty$, with $0 < c_1 \leq 1$. For numerical computations, these boundary conditions were implemented in a finite domain at $x=-L_1$ and $x=L_2$, with L_1 and L_2 increased until there was no effect on the results, which typically required $L_2+L_1 > L$, with $L \in [60,120]$. The initial condition is a flat film $h(x,y,t=0)=1$, which corresponds to an isothermal surface.

III. RESULTS

A. Base profiles

The steady, two-dimensional base profile is found by seeking solutions of the form $h(x,y,t)=h_0(x)$. Making this substitution into Eq. (2) yields

$$\frac{ET_0}{(K+h_0)} + \frac{\partial}{\partial x}[(1+h_{0xxx})h_0^3 - MT_{0x}^i h_0^2] = 0. \tag{7}$$

The base states were computed for a finite domain, $x \in [-L_1, L_2]$, with $h_0(-L_1)=1$, $h_{0xxx}(-L_1)=0$, $h_{0x}(L_2)=0$, and $h_{0xxx}(L_2)=0$. Finite element computations were performed using COMSOL 3.3 to determine the base profiles for a prescribed temperature field $T_0(x)$ at the solid surface using a modified, damped Newton method.[33] The base profile was calculated for a small value of M based on an initial guess value of $h_0=1$, and a continuation method[34] was used to extend the solution to larger values of M. Additional computations were performed by evolving the one-dimensional version of Eq. (2) in time via the method of lines[35] and the implicit DASPK solver[36,37] until a steady profile was obtained, with a unit height profile used for the initial condition. The results were identical to the solution of Eq. (7) as an ordinary differential equation for the cases in which the film does not undergo an oscillatory, thermocapillary instability, as discussed in Sec. III B. The accuracy of the solution method was assessed by checking convergence after mesh refinement, varying the domain length, and examining the invariance of $\int_{-\infty}^{\infty}[MT_x^i/h_0+(1-h_0^3)/h_0^3]dx=0$ for $E=0$. This property is guaranteed from Eq. (7) and its boundary conditions, and the value of this integral was always less than 10^{-9}. Typically, about 2000 points were used for the computations, with local refinement around the regions with steep gradients in the temperature or free-surface shape.

The heater embedded in the substrate is modeled as

$$T_0(x) = 0.5\{\tanh[\omega(x+\chi)] - \tanh[0.5(x-8)]\}, \tag{8}$$

where ω is a parameter that governs the steepness of the temperature increase at the upstream edge of the heater and χ governs the streamwise extent of the heater. It has been shown that ω can have a significant effect on the base profiles and their stability behavior for a volatile liquid and that the oscillatory, thermocapillary instability does not occur if the streamwise width of the heater is sufficiently small.[23] For this study, $\omega=1$ and $\chi=4$.

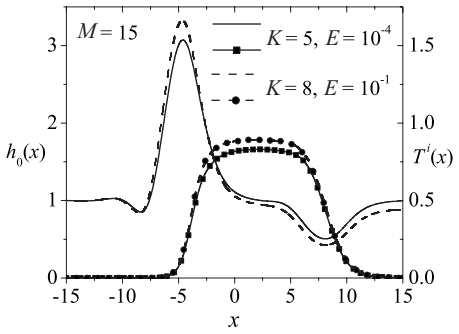

FIG. 2. Base profiles $h_0(x)$ for $M=15$ for different values of K and E. The curves with symbols are the corresponding temperature profiles $T^i(x)$ at the interface.

Base profiles are plotted in Fig. 2 for $M=15$, along with the interfacial temperature in the streamwise direction. At the upstream edge of the heater, the temperature gradient induces a Marangoni stress that opposes the flow of the film, and the film thickens to maintain a constant flow rate. This local thickening is smoothed by surface tension into a pronounced thermocapillary ridge. The amplitude of the ridge increases as M increases. As K decreases, T_x^i decreases, and the amplitude of the ridge decreases because of the smaller Marangoni stress induced by the diminished temperature gradient along the interface. At the downstream edge of the heater, the Marangoni stress augments the flow due to gravity, and the film thins.

B. Linear stability

To investigate the stability of these two-dimensional solutions to perturbations that vary in the transverse direction, the film thickness is perturbed as $h(x,y,t)=h_0(x)+\varepsilon h_1(x,t)\exp(iqy)$, with $\varepsilon \ll 1$ and q the transverse wave number of the perturbation. Upon substitution into Eq. (2) and collecting $O(\varepsilon)$ terms, the linearized equation governing the evolution of perturbations is obtained,

$$\frac{\partial h_1}{\partial t} = \sum_{i=0}^{i=4} \mathbb{L}_i h_1^{(i)}, \tag{9}$$

where

$$\mathbb{L}_0 = -\{3[h_0^2(1+h_{0xxx})]_x - ET_0/(K+h_0)^2 - 2M(T_{0x}^i h_0)_x - M(T_{1x}^i h_0^2)_x + q^2 MT_1^i h_0^2 + q^4 h_0^3\},$$

$$\mathbb{L}_1 = -[3h_0^2(1+h_{0xxx}) - 3q^2 h_0^2 h_{0x} - 2MT_{0x}^i h_0 - MT_{1x}^i h_0^2 - M(T_1^i h_0^2)_x],$$

$$\mathbb{L}_2 = -[-2q^2 h_0^3 - Mh_0^2 T_1^i], \tag{10}$$

$$\mathbb{L}_3 = -3h_0^2 h_{0x},$$

$$\mathbb{L}_4 = -h_0^3.$$

Due to the perturbation in h, the interfacial temperature profile becomes $T^i = T_0^i + \varepsilon h_1 T_1^i$, where $T_0^i(x) = KT_0/(K+h_0)$ and

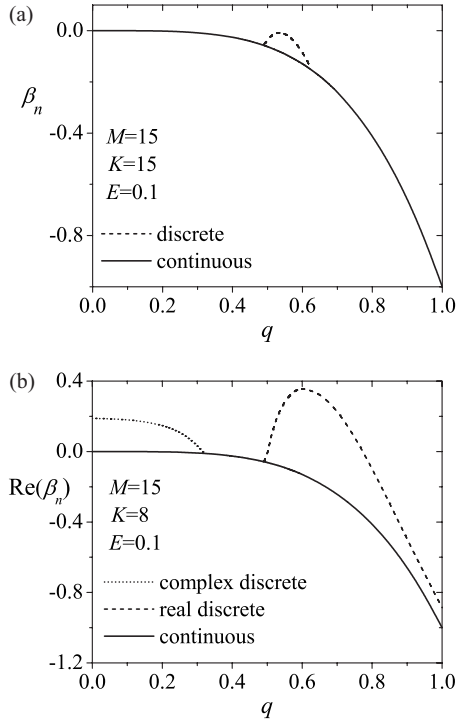

FIG. 3. (a) Leading eigenvalues β_n of **A** for $M=15$, $K=15$, and $E=0.1$. (b) Real part of the leading eigenvalues of **A** for $M=15$, $K=8$, and $E=0.1$.

$T_1^i(x)=-KT_0/(K+h_0)^2$. Equation (9) is solved subject to the boundary conditions

$$h_1 \text{ bounded as } x \to \pm\infty. \tag{11}$$

When discretized in space using fourth-order, centered finite differences, Eqs. (9) and (11) yield a linear system of equations that can be written in vector form as

$$\frac{\partial \boldsymbol{h}_1}{\partial t} = \mathbf{A}\boldsymbol{h}_1, \tag{12}$$

where **A** is an autonomous matrix and $\boldsymbol{h}_1$ is the discretized form of h_1. Assuming exponential time dependence for h_1, $h_1(x,t)=\Phi(x)\exp(\beta t)$, yields the eigenvalue problem $\beta\boldsymbol{\Phi}=\mathbf{A}\boldsymbol{\Phi}$, where $\{\boldsymbol{\Phi}_n\}$ are the n eigenvectors of **A**. For each value of the wave number q, the n eigenvalues $\beta_n(q)$ of the matrix **A** were found using the MATLAB 6.1 function eig. For the domain size and number of grid points used, the leading eigenvalues were insensitive to the size of square matrix **A**, which is of dimension 2000 or larger for all computations.

Representative dispersion curves obtained by solving the eigenvalue problem are shown in Fig. 3 for $M=15$. It was found in a previous study[21] that for $E=0$ and $K\to\infty$, corresponding to a nonvolatile film in the limit of $\mathrm{Bi}\to 0$, the film is stable for $M=15$ and that the leading eigenvalue corresponds to the continuous spectrum given by $\beta=-q^4$. As K is decreased a band of discrete, stable modes appears, as shown in Fig. 3(a) for $K=15$ and $E=0.10$. The discrete modes are real. As K is decreased further, the discrete band extends into the unstable half-plane (for $0.51\le q\le 0.77$) as shown in Fig. 3(b) for $K=8$ and leads to rivulet formation. (Similar behavior occurs as M is increased for fixed K.) It has been shown[21] that the dominant mechanisms for rivulet formation in the limit of small heat loss from the free surface ($K^{-1}=\mathrm{Bi}\to 0$) are the additional capillary pressure gradient due to the perturbation thickness variation in the streamwise direction and gravity. For larger heat loss, the rivulet instability is augmented by a transverse Marangoni flow due to the variation in perturbation thickness.[23] For smaller K, a band of complex, unstable, and discrete modes appears for small q [$0\le q\le 0.31$ in Fig. 3(b)]. These unstable modes correspond to an oscillatory, thermocapillary instability that begins above the heater. The discrete and continuous spectra intersect at $q\approx 0.49$ and $q\approx 0.63$ for the linearly stable film with $K=15$. A more extensive analysis of the structures of these different eigenmodes and the variation of the critical Marangoni number with K and E can be found in the work of Tiwari and Davis.[23]

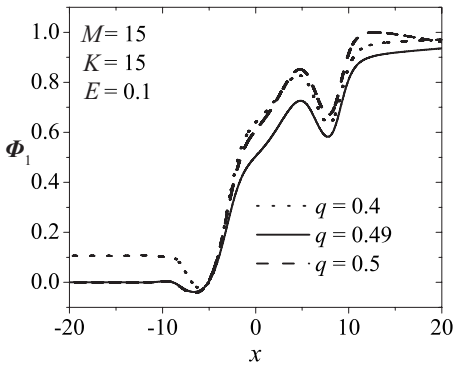

FIG. 4. Leading eigenfunctions for $M=15$, $K=15$, and $E=0.1$.

The dominant eigenvector $\boldsymbol{\Phi}_1$ that corresponds to the leading eigenvalue for $M=15$, $K=15$, and $E=0.1$ is shown in Fig. 4. The continuous mode for $q=0.4$ asymptotes to constant values as $x\to\pm\infty$. For $q=0.5$, the leading eigenfunction is discrete, which corresponds to perturbations localized near the heater and slowly decaying as $x\to\infty$. The wave number $q\approx 0.49$ corresponds to a repeated eigenvalue as the discrete and continuous spectra intersect. The bifurcation of a discrete mode from a resonance pole as it is crossed by the continuous spectrum is discussed in detail by Kalliadasis *et al.*[19] Similar behavior occurs for $q\approx 0.63$.

The nonmodal and nonlinear dynamics of films corresponding to the parameter values in Figs. 3 and 4 are investigated in the remainder of this work to illustrate typical film behavior. The dynamics are similar for other sets of parameter values, including nonvolatile films with $E\to 0$ and $K\equiv \mathrm{Bi}^{-1}$.

C. Transient amplification: Nonmodal analysis

The structure of the base profile is highly nonuniform in space, which when coupled to the nonlinearity of Eq. (2) yields[38,39] a non-normal linear operator **A** with eigenvectors that are not orthogonal. Transient amplification of perturbations due to the interaction of these nonorthogonal eigenvectors could lead to instability wavelengths different than those predicted from a modal linear stability analysis or possibly instability in a linearly stable film due to the large growth of finite-amplitude perturbations at early times.[40,41] Further-

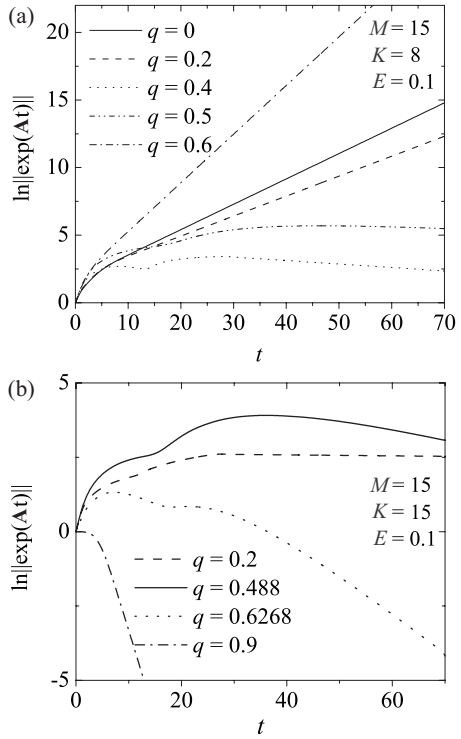

FIG. 5. Maximum transient amplification of spanwise perturbations to the film with $M=15$ and (a) $K=8$ and $E=0.1$ and (b) $K=15$ and $E=0.1$.

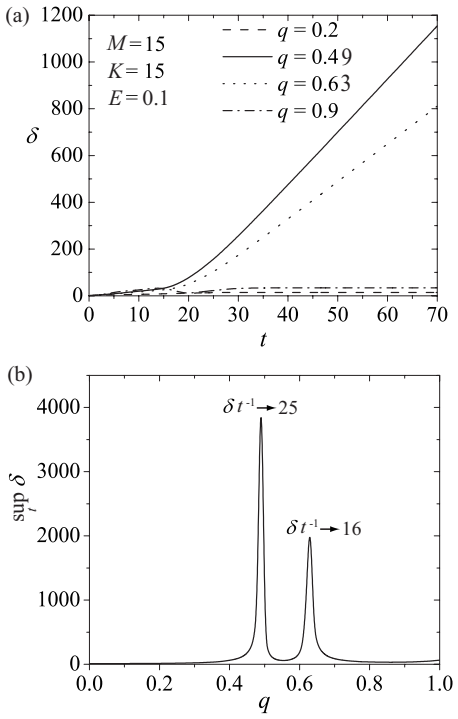

FIG. 6. (a) Maximal nonmodal amplification, $\delta \equiv \|\exp(t\mathbf{A})\|\exp(-\beta t)$, vs t and (b) $\delta(t\to\infty)$ vs q for the linearly stable film with $M=15$, $K=15$, and $E=0.1$.

more, for a normal system, the most harmful perturbation is the leading eigenfunction of the linear system. For a non-normal system, the structure that undergoes the largest amplification, which can be found from a nonmodal analysis, may be significantly different than the eigenfunction and has important implications for techniques to stabilize the flow.

The general solution to Eq. (12) is

$$\boldsymbol{h}_1(t) = \exp(\mathbf{A}t)\boldsymbol{h}_1(t=0), \tag{13}$$

where $\boldsymbol{h}_1(t=0)$ is the initial perturbation applied to the base state. The maximum amplification $\sigma_{\max}$ of an initial perturbation over the time interval t is then given by[41]

$$\sigma_{\max}(t) = \sup_{\boldsymbol{h}_1(t=0)\neq 0} \frac{\|\boldsymbol{h}_1(t)\|}{\|\boldsymbol{h}_1(t=0)\|} = \|\exp(t\mathbf{A})\|, \tag{14}$$

where $\|\cdot\|$ represents the l_2 norm. If nondefective, the matrix $\mathbf{A}$ has the similarity transform $\mathbf{A}=\mathbf{S}\boldsymbol{\Delta}\mathbf{S}^{-1}$, where $\mathbf{S}$ is the matrix whose columns are the normalized eigenvectors $\boldsymbol{\Phi}_n$ of $\mathbf{A}$ in order of growth rate and $\boldsymbol{\Delta}$ is the diagonal matrix of the associated eigenvalues.[42] It follows that

$$\begin{aligned}\exp(\beta_1 t) &\le \|\exp(t\mathbf{A})\| \\ &= \|\mathbf{S}\exp(t\boldsymbol{\Delta})\mathbf{S}^{-1}\| \le \|\mathbf{S}\|\|\mathbf{S}^{-1}\|\exp(\beta_1 t),\end{aligned} \tag{15}$$

where β_1 is the leading entry of $\boldsymbol{\Delta}$, $\{\Delta\}_{11}$. If $\mathbf{A}$ is normal, $\mathbf{S}$ is unitary, and $\|\exp(t\mathbf{A})\|=\exp(\beta_1 t)\ \forall t$. If $\mathbf{A}$ is non-normal, however, the eigenvectors are not orthogonal, and $\|\mathbf{S}\|$ and $\|\mathbf{S}^{-1}\|$ can be very large. Perturbations could therefore be amplified by several orders of magnitude and induce nonlinear effects.[40,41] As $t\to\infty$ the first column of $\mathbf{S}$ and the first row of $\mathbf{S}^{-1}$ exponentially dominate, and it follows from Eqs. (14) and (15) that

$$\lim_{t\to\infty} \sigma_{\max} = \|\boldsymbol{\Phi}_1\|\|\hat{\boldsymbol{\Phi}}_1\|\exp(\beta_1 t), \tag{16}$$

where $\hat{\boldsymbol{\Phi}}_1$ is the leading eigenvector of the adjoint operator associated with $\mathbf{A}$ and normalized such that $\langle\boldsymbol{\Phi}_1,\hat{\boldsymbol{\Phi}}_1\rangle=1$.

The maximum transient amplification of a perturbation to the film is shown in Fig. 5 for two sets of parameter values. Each point on these curves represents the maximum growth of an initial condition that is optimal for the time interval $[0,t)$. In Fig. 5(a), the maximum transient amplification is plotted for $M=15$, $K=8$, and $E=0.1$. The film is unstable for $q=0$, 0.2, and 0.6 and stable for the other wave numbers shown in the plot. Growth rates obtained from the modal analysis were recovered for $t>30$ for $q=0$, 0.2, 0.4, and 0.6. For $q=0.5$, the modal growth rate is not obtained even at $t=70$, and the transient amplification is nearly e^6, which is an indication of the non-normality of $\mathbf{A}$ for this wave number. The maximum transient amplification of perturbations to the linearly stable film for $M=15$, $K=15$, and $E=0.1$ is shown in Fig. 5(b). Transient growth of more than two orders of magnitude is seen for $q=0.2$ and $q=0.49$ even after $t=40$. The large transient growth for $q=q_{r1}\approx 0.49$ is related to the repeated eigenvalue as the discrete and continuous spectra intersect in Fig. 3. Similar transient growth may be expected for $q=q_{r2}\approx 0.63$ where the continuous and discrete spectra also intersect, but the perturbation is amplified less because the model decay rate is larger.

Nonmodal growth can indicate a deviation from the dynamics predicted from the modal analysis. Shown in Fig. 6(a) is the maximum transient amplification with the modal growth factored out, $\delta=\|\exp(t\mathbf{A})\|\exp(-\beta_1 t)$, versus t. For $q=0.2$ and $q=0.9$, this nonmodal growth is less than $O(10)$

and asymptotes to a constant by $t \approx 40$. For $q \approx 0.49$ and $q \approx 0.63$, the nonmodal growth is very large and continues to increase significantly at $t=70$. Shown in Fig. 6(b) is the nonmodal growth at large times, $\delta(t \to \infty) \equiv \|\mathbf{\Phi}_1\| \|\hat{\mathbf{\Phi}}_1\|$, versus q. This quantity is very large for $q=q_{r1}$ and $q=q_{r2}$ for this linearly stable film because $\mathbf{\Phi}_1$ and $\hat{\mathbf{\Phi}}_1$ are nearly orthogonal, although the actual amplification of a perturbation, $\|\exp(t\mathbf{A})\|$, is finite because of the exponential decay associated with the leading eigenvalue. For the repeated eigenvalues at $q=q_{r1}$ and $q=q_{r2}$, the corresponding eigenvectors of $\mathbf{A}$ are identical (within the numerical accuracy), which yields a defective matrix $\mathbf{A}$. The growth rates of the modes are therefore $\exp(\beta_1 t)$ and $t\exp(\beta_1 t)$. The curves δ versus t in Fig. 6 for $q \approx 0.49$ and $q \approx 0.63$ become nearly linear by $t \approx 50$, and $t^{-1}\delta$ asymptotes to a constant value as $t \to \infty$, as indicated in Fig. 6(b). The large transient amplification for $q=q_{r1}$ and $q=q_{r2}$ is therefore due to algebraic growth proportional to t caused by the repeated eigenpair.

These interesting nonmodal dynamics motivate an investigation of the nonlinear dynamics of perturbations to the film. Such large nonmodal growth for the wave numbers corresponding to repeated eigenvalues was also found for linearly unstable films (e.g., $M=15$, $K=8$, and $E=0.1$), although in those cases the dynamics are dominated by the unstable modes. It has been shown that the nonmodal amplification $\delta(t \to \infty)$ is proportional to the square root of the domain length for continuous modes and is independent of the domain length for discrete modes.[21]

D. Optimal perturbations

The evolution of an optimal initial perturbation into its final state after time t can be found by the singular value decomposition[41] of $\exp(t\mathbf{A})$,

$$\exp(t\mathbf{A}) = \mathbf{U}\mathbf{\Sigma}\mathbf{V}^{\dagger}. \tag{17}$$

The columns of the unitary matrix $\mathbf{V}$ are the complete set of (orthogonal) initial states, and the columns of the unitary matrix $\mathbf{U}$ are orthonormal basis vectors that span the range space of final states. The diagonal matrix $\mathbf{\Sigma}$ contains elements σ_i that describe the growth rate of each corresponding initial state during the specified time interval. The vectors $\boldsymbol{V}_i$ form the columns of $\mathbf{V}$, and the optimal perturbation at a specified time, $\boldsymbol{V}_{\text{opt}} \equiv \boldsymbol{V}_1$, is the initial condition that undergoes the maximum growth over the time interval t as it evolves into $\boldsymbol{U}_{\text{opt}}(t)$. This maximum growth is denoted by the leading singular value, $\sigma_{\max}(t) \equiv \|\exp(t\mathbf{A})\|$, and corresponds to the amplification shown in Fig. 5 at time t.

The maximum possible amplification at any time is attained by the optimal initial disturbance calculated for that time. As $t \to \infty$, $\boldsymbol{U}_{\text{opt}}$ asymptotes to the eigenfunction that describes rivulet formation in the spanwise direction, $\mathbf{\Phi}_1$. The optimal initial disturbance, $\boldsymbol{V}_{\text{opt}}(t \to \infty)$, in this long-time limit (at which the most unstable mode dominates) asymptotes to $\hat{\mathbf{\Phi}}_1$, the eigenvector of the adjoint linearized operator, which is the initial condition that optimally excites the most unstable mode. (Slight differences may occur at the ends of the domain due to the imposition of the physical boundary conditions on the adjoint eigenvector.) For normal $\mathbf{A}$, the optimal initial condition for any time is the normalized leading eigenvector.

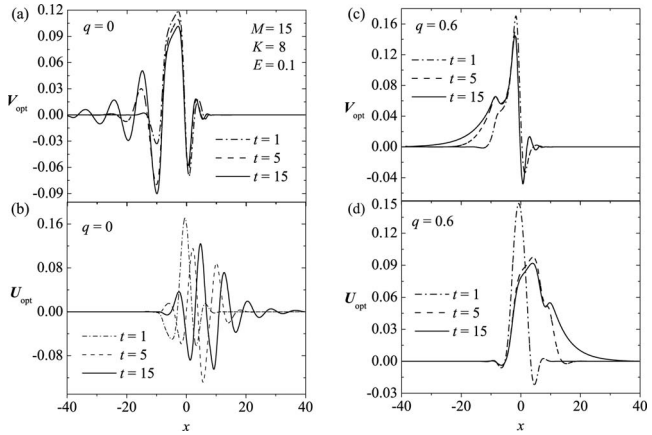

FIG. 7. Optimal perturbations for the unstable base state with $M=15$, $K=8$, and $E=0.1$. (a) Optimal initial perturbation $\boldsymbol{V}_{\text{opt}}$ and (b) corresponding evolved state $\boldsymbol{U}_{\text{opt}}$ after time t for a perturbation with wave number $q=0$. (c) $\boldsymbol{V}_{\text{opt}}$ and (d) $\boldsymbol{U}_{\text{opt}}$ for $q=0.6$.

Shown in Fig. 7 are the optimal initial perturbations and the evolved states for $q=0$ (oscillatory instability) and $q=0.6$ (rivulet instability) with $M=15$, $K=8$, and $E=0.10$. For $q=0$, $\boldsymbol{V}_{\text{opt}}$ is located at the leading edge of the heater for small t and extends a distance $x \approx 20 l_c$ units upstream as decaying oscillations that are convected to the forward portion of the capillary ridge where the Marangoni stress opposes the bulk flow, as shown in Fig. 7(a). By time $t=5$, the oscillations appear at $x \approx -25$. For $t \geq 15$, the oscillations in $\boldsymbol{V}_{\text{opt}}$ extend further upstream such that they undergo transient amplification when they are convected over the heater. For early times, the evolved states $\boldsymbol{U}_{\text{opt}}(t)$ in Fig. 7(b) localize at the upstream edge of the heater but for later times are oscillations that encompass the entire heater by $t=5$ and extend far downstream by $t=15$. By this time $\boldsymbol{U}_{\text{opt}}$ is indistinguishable from the eigenfunction $\mathbf{\Phi}_1$.

The shapes of $\boldsymbol{V}_{\text{opt}}$ and $\boldsymbol{U}_{\text{opt}}$ for $q=0.6$ are plotted in Figs. 7(c) and 7(d) and are significantly different than for $q=0$. For $t=1$, $\boldsymbol{V}_{\text{opt}}$ is sharply peaked at the leading edge of the heater and extends upstream about $x=15 l_c$ units. As t increases, $\boldsymbol{V}_{\text{opt}}$ broadens somewhat upstream but retains the strong peak at the leading edge of the heater. For $t \geq 15$ $\boldsymbol{V}_{\text{opt}}$ is constant in time, and its structure reveals that perturbations applied to the portion of the film from $-40 \leq x \leq 0$ are amplified the most strongly, with the forward portion of the capillary ridge the most sensitive region to perturbations. These results suggest that the rivulet instability might be suppressed by appropriate modulation of the flow in this region of the film. The evolved state $\boldsymbol{U}_{\text{opt}}$ is focused at the forward portion of the capillary ridge (leading edge of the heater). For $t \geq 15$ $\boldsymbol{U}_{\text{opt}}$ is constant and indistinguishable from the leading eigenfunction. This rapid asymptote to the modal behavior corresponds to the small nonmodal growth for unstable q in Fig. 5(a) and occurs because of the near orthogonality between the (discrete) leading eigenfunction and the stable, continuous modes at this value of q.

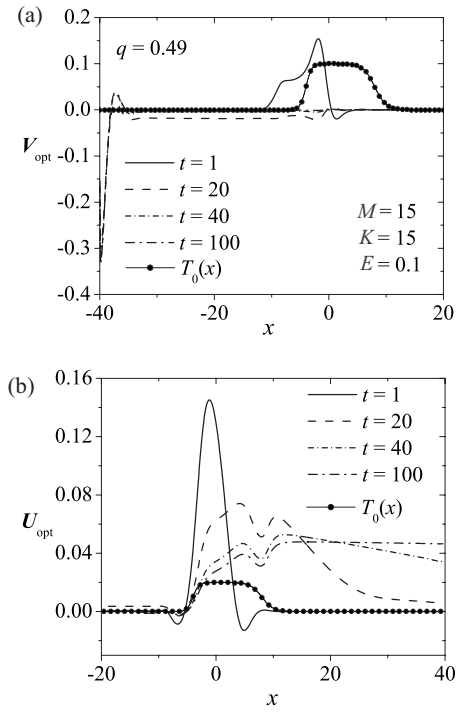

FIG. 8. (a) Optimal initial perturbation $\boldsymbol{V}_{\text{opt}}$ and (b) corresponding evolved state $\boldsymbol{U}_{\text{opt}}$ after time t for a perturbation with wave number $q=0.49$ applied to the linearly stable base state with $M=15$, $K=15$, and $E=0.1$.

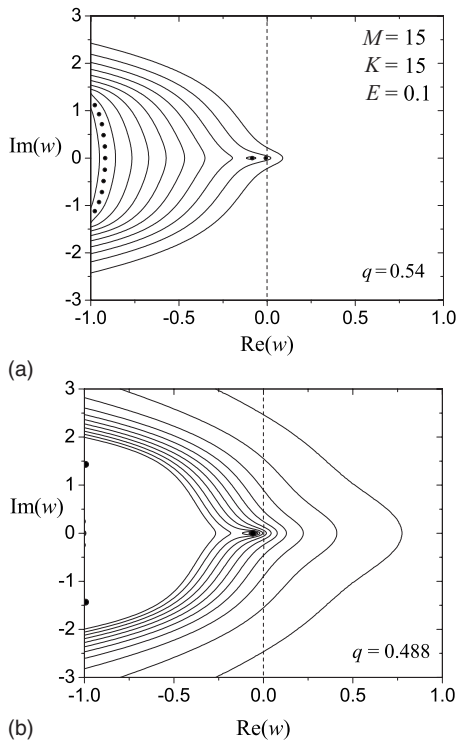

FIG. 9. Plot of the pseudospectra given by $\Lambda_\epsilon(\mathbf{A})=\{w\in\mathbb{C}:w\in\Lambda(\mathbf{A}+\mathbf{E}),\|\mathbf{E}\|\leq\epsilon\}$ for the linearly stable film with $M=15$, $K=15$, $E=0.1$, and (a) $q=0.54$ (least stable eigenvalue) and (b) $q=0.49$ (repeated eigenvalue). The abscissa is Re(w), and the ordinate is Im(w). Contours are plotted for $\epsilon=10^{-1},10^{-2},\ldots,10^{-11}$ [the $\epsilon=10^{-11}$ contour is not visible in (a)]. The symbols are the leading eigenvalues of $\mathbf{A}$.

Shown in Fig. 8 are $\boldsymbol{V}_{\text{opt}}$ and $\boldsymbol{U}_{\text{opt}}$ for $q=0.49$ for the stable film with $M=15$, $K=15$, and $E=0.10$. This wave number corresponds to a repeated eigenvalue, as shown in Fig. 3. At early times $\boldsymbol{V}_{\text{opt}}$ again is peaked at the leading edge of the heater and extends upstream. A more interesting structure appears for intermediate times, $t\approx 20$, at which $\boldsymbol{V}_{\text{opt}}$ extends far upstream like an optimal perturbation for a stable, continuous mode[21] but also has a structure at the leading edge of the heater like an unstable, discrete mode. The shape of $\boldsymbol{V}_{\text{opt}}$ does not change significantly for $t>40$, and the perturbation is focused at the upstream boundary of the computational domain. The evolved perturbation $\boldsymbol{U}_{\text{opt}}$ is again focused at the leading edge of the heater for early t and encompasses more of the film for later t. For earlier times the structure is similar to a discrete mode, but for later times $\boldsymbol{U}_{\text{opt}}$ resembles a stable, continuous mode and eventually asymptotes to the eigenfunction by $t\approx 100$. The deviation from modal dynamics for such an extended time interval after a perturbation is applied implies a significant degree of non-normality in the linear operator and suggests that further investigation of $\mathbf{A}$ is warranted.

E. ϵ-pseudospectra

The ϵ-pseudospectrum of a matrix $\mathbf{A}$ is the set of points[39,40,43]

$$\Lambda_\epsilon(\mathbf{A})=\{w\in\mathbb{C}:w\in\Lambda(\mathbf{A}+\mathbf{E}),\|\mathbf{E}\|\leq\epsilon\}, \tag{18}$$

where $\Lambda(\cdot)$ denotes the spectrum of $(\cdot)$. The ϵ-pseudospectrum thus consists of the eigenvalues of a perturbed matrix and reveals the susceptibility of the eigenvalues to perturbations. For $M=15$, $K=8$, $E=0.1$, and the unstable wave number $q=0.6$, the ϵ-pseudospectral contour does not exceed the spectrum by more than ϵ near the leading eigenvalue, implying that the leading eigenvalue is physically determinant. The minimum angle between the leading eigenvector and each other eigenvector is nearly $\pi/2$, indicating the near orthogonality of the leading eigenmode to the others. The dynamics are thus dominated by the unstable, leading eigenvalue as was also found for unstable films with no heat transfer.[21] The pseudospectra therefore provide little additional information for these parameters and are not shown.

Shown in Fig. 9 are the ϵ-pseudospectra of $\mathbf{A}$ computed with the eigtool (Ref. 44) for MATLAB 6.1. Contours are shown in Fig. 9(a) for $\epsilon=10^{-1},10^{-2},\ldots,10^{-11}$ for the stable film with $M=15$, $K=15$, $E=0.1$, and $q=0.54$, which is the least stable wave number as shown in Fig. 3. The symbols are the leading eigenvalues of $\mathbf{A}$. For each value of ϵ, the ϵ-pseudospectrum extends a distance of approximately ϵ beyond the leading eigenvalue, which is the behavior expected for a normal linear operator. Nonmodal dynamics should therefore be insignificant for $q=0.54$. More interesting is the result for $q=0.49$, which is shown in Fig. 9(b). The film is still stable at this wave number, which corresponds to a repeated eigenvalue. The $\epsilon=10^{-7}$ contour extends into the unstable right half plane [to Re(w)=0.017], indicating that a perturbation to $\mathbf{A}$ with such small magnitude could make the film linearly unstable. In practice, such perturbations could be small deviations of the film profile from that calculated in

Sec. III A due to experimental noise or a minor disruption to the film. The computed eigenvectors corresponding to the repeated eigenvalue are identical, indicating a significant interaction, and the minimum angle between these eigenvectors and the others is greater than $9\pi/25$, so the interaction with those modes is relatively weak. The eigenvalues with nonzero imaginary parts are more susceptible to perturbations because the $\epsilon=10^{-11}$ contours are visible on an $O(1)$ scale at the left of the figure, but these modes do not significantly influence the dynamics because their associated decay rate is much greater. The minimum angle between the other eigenvectors was found to be approximately $\pi/9$, indicating a potential large interaction between the modes that is similar to films with driven contact lines.[38,39] These results suggest that if the linearly stable film were to become unstable due to a finite-amplitude perturbation, instability might occur not for the least stable wave number ($q=0.54$) but instead for the wave number with largest nonmodal growth. This possibility and the relevance of the nonmodal analysis to the nonlinear dynamics are explored in Sec. III F.

F. Nonlinear evolution of perturbations

Computations with Eq. (2) were performed to study the nonlinear evolution of perturbations and the significance of the nonmodal dynamics. After computing the steady base state, a perturbation was applied to the film, and its evolution was computed using periodic boundary conditions in y and the conditions given by Eq. (6) in x. Soft boundary conditions[45,46] were used at $x=L_2$ and were found to have a negligible effect away from the boundary. The perturbation was chosen to be the structure with the maximum instantaneous growth rate, which can be found from eigenanalysis of the matrix $\mathbf{B}=(\mathbf{A}+\mathbf{A}^{\dagger})/2$. This growth rate is the leading eigenvalue (the spectral abscissa) of $\mathbf{B}$, $\lambda_{\max}^{R}(\mathbf{B}) \equiv \max\{\Lambda(\mathbf{B})\}$, and the perturbation that induces this growth is the corresponding eigenvector $\mathbf{\Phi_B}$. This instantaneous growth rate is also a nonlinearly valid bound on the potential for perturbation growth.[41,47]

Shown in Fig. 10(a) is the maximum instantaneous growth rate, $\alpha(\mathbf{A}) \equiv \lambda_{\max}^{R}(\mathbf{B})$, for $M=15$, $E=0.1$, and several values of K. As K increases, α decreases, which is the same trend as in the linear stability results. Shown in Fig. 10(b) are the corresponding eigenvectors $\mathbf{\Phi_B}$ for $K=15$ and $q=0$, $q=0.49$, and $q=0.63$. The perturbations are again localized at the leading edge of the heater and forward portion of the fluid ridge.

As a check on the nonlinear computations, the linear stability results were first verified. The growth of the perturbation is defined as the amplification ratio $H=\ln[\|h(x,y,t)-h_0(x)\|/\|h(x,y,t=0)-h_0(x)\|]$, where $\|(\cdot)\| = [\iint_{\mathrm{CD}}(\cdot)^2 dxdy]^{1/2}$ and CD represents the computational domain. The initial perturbation is $\mathbf{\Phi_B}\cos(qy)$, and its magnitude is $\varepsilon_1=\|h(x,y,t=0)-h_0(x)\|$, which is comparable to the maximum amplitude of the perturbation. The domain width in y for these computations is $2\pi/q$.

The nonlinear growth of a perturbation for the linearly unstable film with $M=15$, $K=8$, and $E=0.1$ is shown in Fig. 11(a). For $q=0.6$ it can be seen from Fig. 3 that the film is linearly unstable with eigenvalue $\beta=0.34$. After a brief transient period, the slope of the curve for $q=0.6$ in Fig. 11(a) is 0.335 until $t\approx 20$, which is in good agreement with the linear stability result. After this time the slope increases as the film thins significantly between the developing rivulets. A contour plot of the computed film profile after rivulet formation is shown for these parameters in Fig. 11(b). The rivulets extend from the thermocapillary ridge and are separated by thin regions of the film. At later times the film thins and tends to rupture at the front of the thermocapillary ridge due to the mass loss above the heater. It was found that rupture could be prevented through the introduction of a disjoining pressure term in the evolution equation, but the dynamics as the film thins significantly between the rivulets is beyond the scope of this work. For $q=0.35$, the film is stable for $\varepsilon_1<10^{-3}$ as predicted by the linear stability analysis, and the growth of a small perturbation is shown by the curve with an s in the plot. For perturbations with $\varepsilon_1>10^{-3}$, the film is nonlinearly unstable, and the growth of such an unstable perturbation is given by the curve with a u. Also plotted is the growth of the perturbation for $q=0$, which in the linear stability analysis has a complex eigenvalue with positive real part. It is apparent from the nonlinear results that this oscillatory thermocapillary instability evolves to a new two-dimensional, time-periodic base state. This transition is associated with a Hopf bifurcation from the steady base state as M is increased or as K is decreased. The growth rate before nonlinear saturation is consistent with the prediction of the linear stability analysis. This time-periodic base state is examined further in Sec. III G.

A linear combination of perturbations of different wave numbers $0.25<q<1.0$ with $\varepsilon_1=10^{-2}$ was applied to the base

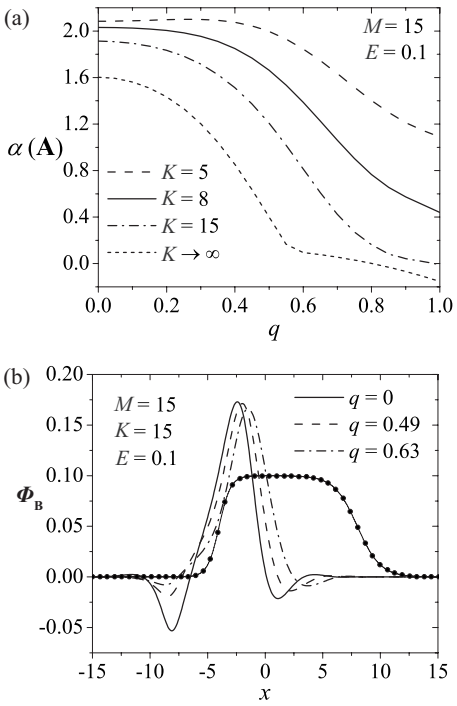

FIG. 10. (a) Maximum instantaneous growth rate $\alpha(\mathbf{A})$ vs q for $M=15$, $E=0.1$, and several K. (b) Corresponding eigenvectors $\mathbf{\Phi_B}$ for $M=15$, $K=15$, and $E=0.1$. The curve with symbols is $T_0(x)$.

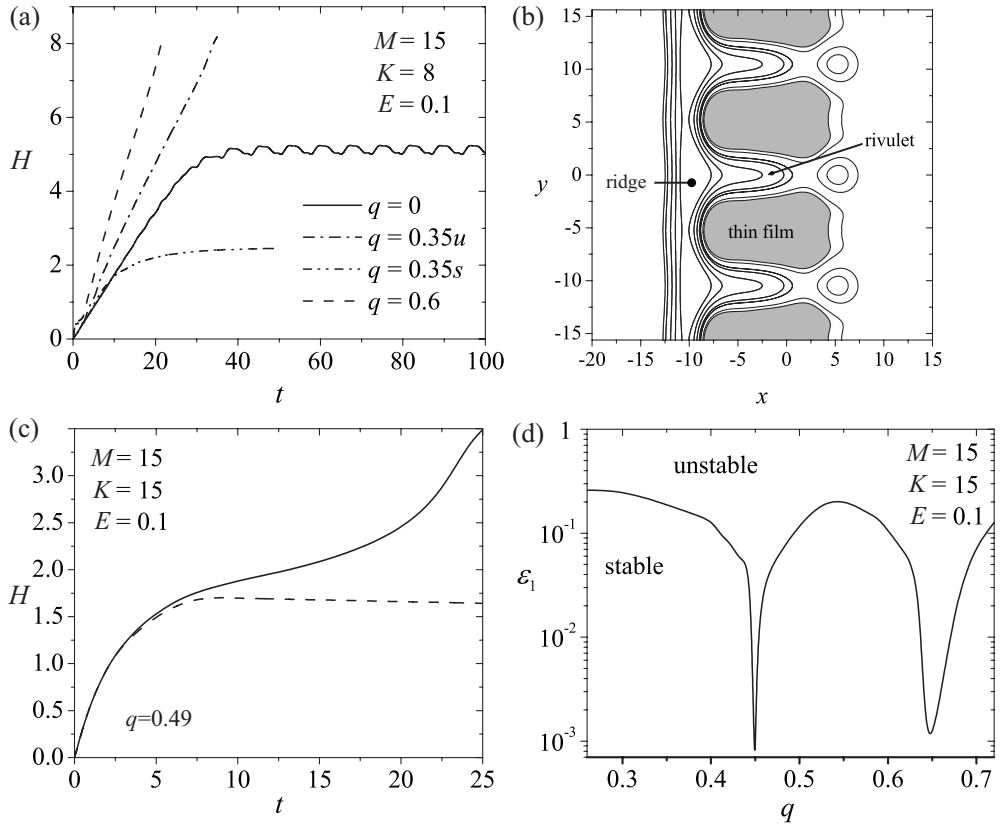

FIG. 11. (a) Nonlinear amplification ratio H of perturbations to the linearly unstable film with $M=15$, $K=8$, and $E=0.1$. (b) Contour plot of $h(x,y,t)$ of the nonlinear film evolution after rivulet formation. Contours are shown for $h=0.5$, 0.75, 1.25, 1.5, 2.0, 2.5, and 3.0. (c) Nonlinear amplification ratio H for the linearly stable film with $M=15$, $K=15$, and $E=0.1$. (d) Magnitude of perturbation ε_1 that destabilizes the linearly stable film with $M=15$, $K=15$, and $E=0.1$.

state with the parameter values in Fig. 11(a), and an array of rivulets ultimately developed for this linearly unstable flow with the transverse wave number that corresponds to the largest eigenvalue, confirming that the linear stability results capture the relevant dynamics for this linearly unstable flow. Further, the oscillatory, thermocapillary instability developed for $K=5$ for a similar linear combination of small perturbations, which is consistent with the linear stability results for that value of K. The width of the computational domain was twice the longest wavelength of the applied perturbations.

Shown in Fig. 11(c) are the nonlinear growth curves for the linearly stable film with $M=15$, $K=15$, $E=0.1$, and $q=0.49$. For very small ε_1, there is a period of transient growth, after which the perturbation decays at the rate predicted from the linear stability analysis. For perturbations of $O(10^{-3})$ or larger, however, the film is nonlinearly unstable. The increase in the growth rate for $t>20$ corresponds to rapid rivulet formation. The magnitude of the perturbation needed to induce a nonlinear instability in this linearly stable film (for the particular choice of initial perturbations) is shown in Fig. 11(d). Instability was found for very small perturbations with $\varepsilon_1<10^{-3}$ for two particular wave numbers: $q\approx0.49$ and $q\approx0.63$. These two values correspond to the wave numbers in Fig. 6 at which the nonmodal growth is very large due to the repeated eigenvalue. The nonmodal analysis of the linearized operator thus predicts the wave numbers at which the nonlinear effects can be important. For $q>0.8$, the film was linearly stable even for perturbations of $O(1)$. A linear combination of perturbations of various wave numbers (including $q\approx0.54$, which corresponds to the least stable eigenvalue) was applied to the film with $\varepsilon_1=10^{-2}$ for each perturbation, and the rivulet instability developed with a wavelength of $q\approx0.49$. Although very large nonmodal growth is also predicted for $q=0.63$, the modal decay rate is larger than for $q=0.49$, which explains the preferred wavelength for pattern formation.

The method of normal forms[48–50] could provide additional qualitative information about the weakly nonlinear dynamics near the instability threshold of this non-normal linear system.[51] For example, for thin liquid films with spatially nonuniform base states, a weakly nonlinear stability analysis of the (long-wave) fingering instability in gravity-driven films with moving contact lines has been performed using a center manifold projection to obtain a Kuramoto–Sivashinsky-type equation,[52] and the dynamics in that case was dominated by the neutrally stable mode corresponding to $q=0$. In the present case, however, the transient amplification of perturbations is large for a narrow band of wave numbers separated from zero and only for $M_c<M<M_{\text{crit}}$ with $(M_{\text{crit}}-M_c)/M_{\text{crit}}\ll1$. The nonmodal growth is small for $M<M_c$, and the dynamics is dominated by the unstable mode for $M>M_{\text{crit}}$. A weakly nonlinear analysis is therefore left as a topic for future study.

Nonlinear simulations for a nonvolatile film ($E=0$) were also performed. It was reported in the work of Tiwari and Davis[21] that for $M=25$ and $\mathrm{Bi}\to 0$ the film is unstable, with the largest eigenvalue corresponding to $q=0.4$. For a linear combination of perturbations with different wave numbers, $q=0.4$ was selected. Instability occurred at this wave number even when the base state was perturbed by a superposition of 20 modes with different wave numbers with a random amplitude in the range $\varepsilon_1<0.05$. For $M=19.9$, the film was nonlinearly stable even for $\varepsilon_1=0.5$, which confirms the linear stability analysis that predicted instability for $M>M_{\mathrm{crit}}=19.9$. Note that for a linearly stable film in the limit $\mathrm{Bi}\to 0$, discrete modes do not exist for relevant values of q, as discrete modes appear only when the film becomes linearly unstable. (By contrast, for a volatile film or with $\mathrm{Bi}>0$, a linearly stable film has a band of discrete modes for $M_c<M<M_{\mathrm{crit}}$, where M_c is slightly less than M_{crit}.[23]) The interesting nonmodal dynamics and nonlinear instability of a linearly stable film for small ε_1 are associated with the presence of discrete modes with the (real) eigenvalue for the discrete modes larger than that for the continuous spectrum ($\beta=-q^4$). For example, for a nonvolatile film with $M=21$ and $\mathrm{Bi}=0$, discrete modes appear for $q\in[0.32,0.46]$. Linearly unstable discrete modes were found for $q\in[0.35,0.44]$. Linearly stable modes appear for $q\in[0.32,0.35)$ and $q\in(0.44,0.46]$, and the film is nonlinearly unstable at these wave numbers for $\varepsilon_1=O(10^{-4})$. (Since stable discrete modes only appear for a linearly unstable film with $E=0$ and $\mathrm{Bi}\to 0$, when there are also linearly unstable modes, the unstable eigenvalues dominate. Without discrete modes, there is minimal transient growth. In this limit, therefore, the nonlinear dynamics do not deviate strongly from the predictions of eigenvalue analysis.[21]) The film was stable in the nonlinear simulations for $q>0.46$ even for a perturbation of magnitude $\varepsilon_1=0.5$, which is expected because the spectral abscissa for these wave numbers corresponds to the continuous spectrum. The nonmodal and nonlinear dynamics are much less significant when the discrete modes have a faster decay rate than the leading part of the continuous spectrum. Because $(M_{\mathrm{crit}}-M_c)/M_{\mathrm{crit}}\ll 1$ for the volatile film, eigenanalysis should provide an accurate prediction of the behavior of small perturbations and the film's stability for most of the conditions of interest.

G. Bifurcation to time-periodic base state

As discussed in Sec. III F, the oscillatory, thermocapillary instability predicted from a linear stability analysis of the steady base state for $q=0$ evolves nonlinearly into a new, time-periodic base state $h_p(x,t)$ that is uniform in the transverse direction. With a pair of complex conjugate eigenvalues $\beta_{1,2}$ with $\Re\mathrm{e}[\beta_{1,2}(q=0)]\to 0$ as $M\to M^*=13.225$ for $K=8$ and $E=0.10$ and with $d/dM\{\Re\mathrm{e}[\beta_{1,2}(q=0)]\}|_{M=M^*}=0.098>0$, this transition corresponds to a Hopf bifurcation and occurs for sufficiently small K. When the heat loss from the free surface is sufficiently large, T^i varies significantly with the local film thickness. A small variation of h with x therefore induces a Marangoni stress from thinner (warmer) to thicker (cooler) regions of the film above the heater. The interaction of this Marangoni stress with gravity and, to a lesser extent, the streamwise capillary flow from variations in the film curvature results in the oscillatory behavior.[23]

To examine the nonlinear dynamics, after the steady base state $h_0(x)$ was computed, a small perturbation was applied to the film and then evolved in time. Shown in Fig. 12(a) is the evolution of the film near the heater at early times after the perturbation is applied for $M=15$, $K=8$, and $E=0.1$. The perturbation is the eigenfunction for $q=0$ found from the linear stability analysis, and its magnitude is $\varepsilon_1=0.01$. (It was verified that instability develops for ε_1 that is orders of magnitude smaller, but the time required for nonlinear saturation is significantly greater.) After the perturbation is applied at $t=0$, the film begins to oscillate above the heater, with the amplitude (and period) of oscillations slowly growing in time. As they grow, the oscillations extend into the film beyond the heater.

Once the oscillations grow sufficiently large that the film thins significantly above the heater, the amplitude of the capillary ridge is affected, much as for spreading films with moving contact lines, for which it has been shown that the amplitude of the ridge increases as the thickness of the precursor film ahead of it decreases.[53–57] The oscillations then include the ridge, are largest above the heater, and decay as they are convected downstream of the heater as waves. Shown in Fig. 12(b) are the film profiles at intervals of 1 time unit after the time-periodic state $h_p(x,t)$ is reached. For these parameter values, the period is approximately 7.32. The dark solid line is the steady base profile, and the dashed lines denote the minimum and maximum values of the film thickness attained at each value of x.

Phase space plots of $\partial h_p/\partial t$ versus h_p are shown in Fig. 12(c) at four x-locations. At $x=20$, which is downstream of the heater, the variations in h_p are relatively small and occur more slowly than at locations further upstream. The variations in h_p are significant at $x=0$, which is above the heater. At $x=10$, which is just downstream of the heater, the variations in the film are less pronounced, but the film thickness varies rapidly.

The waves that are formed due to the oscillations also affect the rate of heat transfer from the heated surface to the film. The dimensionless heat transfer coefficient in the flowing film is defined as

$$\mathrm{Bi}_f \equiv \frac{k_{\mathrm{heat}}\hat{h}_\infty}{k} = \int_{x_1}^{x_2}\left[\frac{-k(\partial\hat{T}/\partial\hat{z})|_{\hat{z}=0}}{\hat{T}_0-\hat{T}^i}\right]\frac{\hat{h}_\infty}{k}dx = \int_{x_1}^{x_2}\frac{1}{h}dx, \tag{19}$$

where k_{heat} is the convective heat transfer coefficient in the film and x_2-x_1 is the width of the heater [determined from $T_0(x_i)=0.01$, $i=1,2$]. The heat transfer coefficient relative to that for the steady flow, $\mathrm{Bi}_{\mathrm{film}}=\mathrm{Bi}_{\mathrm{osc}}/\mathrm{Bi}_{\mathrm{SS}}$, is plotted in Fig. 12(d) for profiles with the time interval $\Delta t=1$. Heat transfer to the film is significantly increased by the waves, with the average over one period about twice as large as for the steady flow. An even larger heat transfer coefficient has been calculated for flow over a surface with a periodic temperature profile.[11]

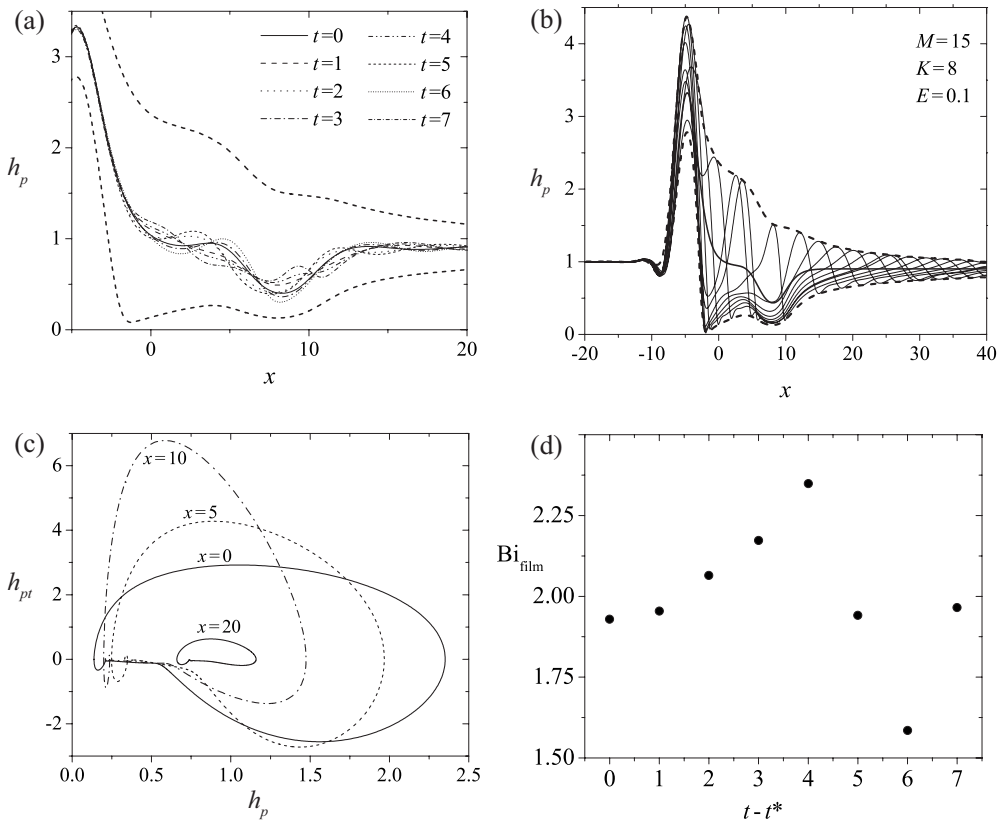

FIG. 12. (a) Oscillations above the heater after a perturbation is applied to the steady film profile $h_0(x)$ at $t=0$. The dashed curves indicate the maximum and minimum values of the film thickness after the oscillations evolve into a time-periodic profile. (b) Profiles at intervals of $\Delta t=1$ after the film reaches the time-periodic state. The dark curve is the steady base state. (c) Phase space plots at $x=0,5,10,20$. (d) Dimensionless heat transfer coefficient after the time-periodic state is reached relative to that for the steady profile at intervals of $\Delta t=1$.

While these time-periodic profiles enhance the heat transfer rate, which is desirable for some applications, it is also of interest to examine their stability to transverse perturbations. A linear stability analysis of the time-periodic profile $h_p(x,t)$ was performed by expressing the film thickness as $h(x,y,t)=h_p(x,t)+h_{p1}(x,t)\cos(qy)$ with $\|h_{p1}\| \ll \|h_p\|$. The time-periodic base state was evolved along with Eq. (9), which is the linearized equation governing the evolution of perturbations that vary sinusoidally in the transverse direction with wave number q. Both uniform and Gaussian initial conditions were used for $h_1(t=0)$, and the results after several periods of evolution were found to be independent of the initial condition used. The asymptotic, exponential growth rate of the perturbations (within the linearized analysis) is

$$\beta_L = \lim_{t\to\infty} \sup\, t^{-1} \ln \frac{\|h_{p1}(x,t)\|}{\|h_{p1}(x,t=0)\|}. \tag{20}$$

This quantity is similar to the first Lyapunov exponent except that the formal propagator[58] (based on a time-ordered exponential) is not used.

Shown in Fig. 13 is the effective dispersion curve β_L versus q for the time-periodic base profile with $M=15$, $K=8$, and $E=0.1$. This time-periodic profile is also unstable to spanwise perturbations. The maximum growth rate occurs for $q\approx 0.4$, which corresponds to a perturbation wavelength about 50% larger than for the steady base state with these same parameter values, and the exponential growth rate is three times larger. As shown in Fig. 3, the steady film is stable for $0.32\leq q\leq 0.50$ and for $0.78\leq q$, whereas the time-periodic film is unstable for $0<q\leq 0.73$. The resulting unsteady film profiles, which are waves in the streamwise direction that undulate in the transverse direction, are reminiscent of inertial waves modulated by Marangoni stresses in films flowing over locally heated surfaces,[59,60] although in the present case inertial effects are insignificant, and the waves decay in amplitude as they are convected far downstream of the heater.

It has been confirmed by explicit computation that all of the results in Sec. III G also occur for a nonvolatile film with

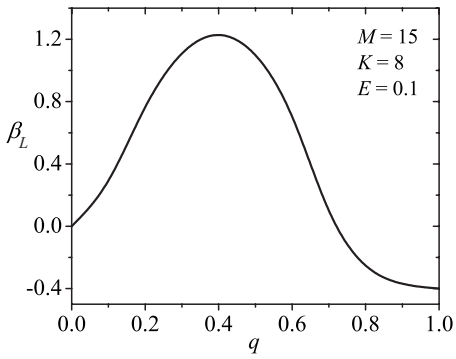

FIG. 13. Asymptotic exponential growth rate of transverse perturbations to the time-periodic film.

$E=0$ and $\mathrm{Bi}=K^{-1}>0$. For example, for $M=15$, $K=\mathrm{Bi}^{-1}=9$, and $E=0$, for which the leading eigenvalues for $q=0$ are $0.0085\pm 2.17i$, the instability begins as small oscillations over the heater with a period of approximately 2.9. The oscillations increase slowly in amplitude (because the spectral abscissa is rather small) and eventually evolve into a profile very similar to that shown in Fig. 12. Once the oscillations extend beyond the heater and encompass the capillary ridge, they become waves that decay as they are convected along the film, and the effective oscillation period increases until the time-periodic state is reached with a period of 5.3. The time-periodic state of this nonvolatile film is also susceptible to a transverse instability.

IV. CONCLUSION

The stability of a thin, volatile liquid film falling under the influence of gravity down a locally heated plate was analyzed in the noninertial regime using a model based on long-wave theory. Because the linearized operator that governs the evolution of perturbations is non-normal, the rivulet and thermocapillary instabilities that develop were investigated using a transient, nonmodal analysis and nonlinear computations of the evolution of perturbations to the film.

The nonmodal analysis identified the upstream edge of the heater and downstream edge of the capillary ridge as the regions of the film that are the most sensitive to perturbations. Very large nonmodal amplification was found for perturbations with wave numbers that correspond to the intersection of the discrete and continuous spectra. Computations of the pseudospectra of the governing linearized operator further suggested the importance of nonmodal effects for these wave numbers, as the magnitude of the perturbation (to the linear operator) required to destabilize a linearly stable flow was found to be several orders of magnitude smaller than for the wave number corresponding to the eigenvalue with largest real part. The possible importance of these effects was confirmed by computations of the nonlinear dynamics, which revealed that for $M_c<M<M_{\mathrm{crit}}$, small perturbations can be sufficient to destabilize a linearly stable film for a narrow band of wave numbers predicted by the nonmodal analysis. The importance of the transient and nonlinear effects was linked to the presence of a band of stable, discrete modes.

Furthermore, the thermocapillary instability was found to lead to a time-periodic, two-dimensional base state that corresponds to a Hopf bifurcation as M is increased or K is decreased. A linear stability analysis of this time-periodic state was performed and reveals further instability to transverse perturbations. The wavelength of the most unstable mode is about 50% smaller than for the rivulet instability of the steady base state, the exponential growth rate is three times larger, and the time-periodic flow is unstable to perturbations with a large range of wave numbers for which the steady base state is stable. The resulting behavior after instability onset is reminiscent of inertial waves on locally heated films, although the wave amplitude is larger in the present case near the heater and decays downstream where the Marangoni stress vanishes. The dimensionless heat transfer coefficient that characterizes heat transfer from the heated surface to the flowing film was found to more than double upon the transition to the time-periodic flow. These results for a volatile film were found to occur also for a nonvolatile film with sufficiently large Biot number characterizing the heat loss from the liquid-gas interface.

While thin liquid films that flow over topographical features develop similar capillary ridges to those in flow over locally heated substrates, the transient amplification of perturbations was found to be insignificant in that system.[61] For the system with topography, a linear stability analysis predicts that the film is stable for a wide range of the pertinent parameters.[62] The operator of the linearized system has a continuous spectrum for disturbances with wave numbers less than a critical value. The discrete spectrum exists only above this critical wave number, and the associated decay rate of the disturbances is extremely rapid because surface tension damps these highly oscillatory perturbations. For the smaller wave numbers with slower decay rates, disturbances cannot localize at the capillary ridge because of the lack of a discrete spectrum, so they are simply convected away by the flow. The perturbation dynamics are therefore similar in the system with localized heating only for sufficiently small values of M and large values of K that discrete modes do not exist.

In addition to variations in topography and temperature, surface heterogeneity often occurs from lateral gradients in wettability, which can significantly influence the dynamics of liquid films and drops. Recent theoretical studies have shown that the depinning of two-dimensional[63,64] (ridges) and three-dimensional[65] drops from a locally wetting or dewetting stripe involves fascinating dynamics, and saddle-node and Hopf bifurcations have been predicted. It is of interest in future work to apply the analysis in this present paper to the depinning problem and the bifurcation analysis to the present problem involving the locally heated stripe to provide further insight, as real substrates may have a combination of local chemical or topographical defects and temperature gradients.

ACKNOWLEDGMENTS

J.M.D. kindly acknowledges support from the 3M Co., NSF CAREER Award No. CBET-0644777, and a Camille Dreyfus Teacher-Scholar Award.

[1] A. Oron, S. H. Davis, and S. G. Bankoff, "Long-scale evolution of thin liquid films," Rev. Mod. Phys. **69**, 931 (1997).
[2] S. H. Davis, "Thermocapillary instabilities," Annu. Rev. Fluid Mech. **19**, 403 (1987).
[3] M. F. Schatz and G. P. Neitzel, "Experiments on thermocapillary instabilities," Annu. Rev. Fluid Mech. **33**, 93 (2001).
[4] E. Ya. Gatapova and O. A. Kabov, "Shear-driven flows of locally heated liquid films," Int. J. Heat Mass Transfer **51**, 4797 (2008).
[5] J. Margerit, P. Colinet, G. Lebon, C. S. Iorio, and J. C. Legros, "Interfacial nonequilibrium and Benard–Marangoni instability of a liquid-vapor system," Phys. Rev. E **68**, 041601 (2003).
[6] J. P. Burelbach, S. G. Bankoff, and S. H. Davis, "Nonlinear stability of evaporating/condensing liquid films," J. Fluid Mech. **195**, 463 (1988).
[7] S. W. Joo, S. H. Davis, and S. G. Bankoff, "Long wave instabilities of heated films: Two dimensional theory of uniform layers," J. Fluid Mech. **230**, 117 (1991).

[8]S. W. Joo, S. H. Davis, and S. G. Bankoff, "A mechanism for rivulet formation in heated films," J. Fluid Mech. **321**, 279 (1996).
[9]S. Kalliadasis, E. A. Demekhin, C. Ruyer-Quil, and M. G. Velarde, "Thermocapillary instability and wave formation on a film falling down a uniformly heated plane," J. Fluid Mech. **492**, 303 (2003).
[10]B. Scheid, C. Ruyer-Quil, S. Kalliadasis, M. G. Velarde, and R. K. Zeytounian, "Thermocapillary long waves in a liquid film flow. Part 2. Linear stability and nonlinear waves," J. Fluid Mech. **538**, 223 (2005).
[11]B. Scheid, A. Oron, P. Colinet, U. Thiele, and J. C. Legros, "Nonlinear evolution of nonuniformly heated falling liquid films," Phys. Fluids **14**, 4130 (2002).
[12]S. Miladinova, S. Slavtchev, G. Lebon, and J. C. Legros, "Long-wave instabilities of non-uniformly heated falling films," J. Fluid Mech. **453**, 153 (2002).
[13]S. Miladinova, D. Staykova, G. Lebon, and B. Scheid, "Effect of nonuniform wall heating on the three-dimensional instability of falling films," Acta Mech. **156**, 79 (2002).
[14]S. Miladinova and G. Lebon, "Effects of nonuniform heating and thermocapillarity in evaporating films falling down an inclined plate," Acta Mech. **174**, 33 (2005).
[15]E. A. Demekhin, S. Kalliadasis, and M. G. Velarde, "Suppressing falling film instabilities by Marangoni forces," Phys. Fluids **18**, 042111 (2006).
[16]I. V. Marchuk and O. A. Kabov, "Numerical modeling of thermocapillary reverse flow in thin liquid films under local heating," Russ. J. Eng. Thermophys. **8**, 17 (1998).
[17]O. A. Kabov, J. C. Legros, I. V. Marchuk, and B. Scheid, "Deformation of free surface in a moving locally-heated thin liquid layer," Fluid Dyn. **36**, 521 (2001).
[18]J. M. Skotheim, U. Thiele, and B. Scheid, "On the instability of a falling film due to localized heating," J. Fluid Mech. **475**, 1 (2003).
[19]S. Kalliadasis, A. Kiyashko, and E. A. Demekhin, "Marangoni instability of a thin liquid film heated from below by a local heat source," J. Fluid Mech. **475**, 377 (2003).
[20]A. M. Frank and O. A. Kabov, "Thermocapillary structure formation in a falling film: Experiment and calculations," Phys. Fluids **18**, 032107 (2006).
[21]N. Tiwari, Z. Mester, and J. M. Davis, "Stability and transient dynamics of thin liquid films flowing over locally heated surfaces," Phys. Rev. E **76**, 056306 (2007).
[22]Yu. O. Kabova, V. V. Kuznetsov, and O. A. Kabov, "The effect of mutual location of heaters on the falling film dynamics," Microgravity Sci. Technol. **19**, 53 (2007).
[23]N. Tiwari and J. M. Davis, "Linear stability of a volatile liquid film flowing over a locally heated surface," Phys. Fluids **21**, 022105 (2009).
[24]O. A. Kabov, "Heat transfer from a small heater to a falling liquid film," Heat Transfer Res. **27**, 221 (1996).
[25]O. A. Kabov, I. V. Marchuk, and V. M. Chupin, "Thermal imaging study of the liquid film flowing on a vertical surface with local heat source," Russ. J. Eng. Thermophys. **6**, 105 (1996).
[26]O. A. Kabov, "Formation of regular structures in a falling liquid film upon local heating," Thermophys. Aeromechanics **5**, 547 (1998).
[27]O. A. Kabov, I. V. Marchuk, A. V. Muzykantov, J. C. Legros, E. Istasse, and J. L. Dewandel, in *Proceedings of the Second International Symposium on Two-Phase Flow Modelling and Experimentation*, edited by G. P. Celata, P. DiMarco, and R. K. Shah (Edizioni ETS, Pisa, Italy, 1999), Vol. 2, pp. 1225–1233.
[28]J. R. Maa, "Evaporation coefficients of liquids," Ind. Eng. Chem. Fundam. **6**, 504 (1967).
[29]H. J. Palmer, "The hydrodynamic stability of rapidly evaporating liquids at reduced pressure," J. Fluid Mech. **75**, 487 (1976).
[30]R. Marek and J. Straub, "Analysis of the evaporation coefficient and the condensation coefficient of water," Int. J. Heat Mass Transfer **44**, 39 (2001).
[31]C. A. Ward and D. Stanga, "Interfacial conditions during evaporation or condensation of water," Phys. Rev. E **64**, 051509 (2001).
[32]E. Sultan, A. Boudaoud, and M. B. Amar, "Evaporation of thin film: Diffusion of the vapor and Marangoni instabilities," J. Fluid Mech. **543**, 183 (2005).
[33]P. Deuflhard, "A modified Newton method for the solution of ill-conditioned systems of nonlinear equations with application to multiple shooting," Numer. Math. **22**, 289 (1974).
[34]P. Deuflhard, "A stepsize control for continuation methods and its special application to multiple shooting techniques," Numer. Math. **33**, 115 (1979).
[35]W. E. Schiesser, *The Numerical Method of Lines* (Academic, San Diego, 1991).
[36]K. E. Brennan, S. L. Campbell, and L. R. Petzold, *Numerical Solution of Initial-Value Problems in Differential-Algebraic Equations* (Elsevier, New York, 1989).
[37]P. N. Brown, A. C. Hindmarch, and L. R. Petzoid, "Using Krylov methods in the solution of large-scale differential-algebraic systems," SIAM J. Sci. Comput. (USA) **15**, 1467 (1994).
[38]J. M. Davis and S. M. Troian, "On a generalized approach to the linear stability of spatially nonuniform thin film flows," Phys. Fluids **15**, 1344 (2003).
[39]J. M. Davis and S. M. Troian, "Influence of boundary slip on the optimal excitations in thermocapillary driven spreading," Phys. Rev. E **70**, 046309 (2004).
[40]L. N. Trefethen, A. E. Trefethen, S. C. Reddy, and T. A. Driscoll, "Hydrodynamic stability without eigenvalues," Science **261**, 578 (1993).
[41]B. F. Farrell and P. J. Ioannou, "Generalized stability theory. Part 1: Autonomous operators," J. Atmos. Sci. **53**, 2025 (1996).
[42]G. H. Golub and C. F. V. Loan, *Matrix Computations*, 2nd ed. (Johns Hopkins University Press, Baltimore, MD, 1990).
[43]L. N. Trefethen, in *Pseudospectra of Matrices, Numerical Analysis 1991*, edited by D. F. Griffiths and G. A. Watson (Longman Scientific and Technical, Harlow, Essex, UK, 1992), pp. 234–266.
[44]T. G. Wright and L. N. Trefethen, "Large-scale computation of pseudospectra using ARPACK and eigs," SIAM J. Sci. Comput. (USA) **23**, 591 (2001).
[45]H.-C. Chang, E. A. Demekhin, and S. S. Saprikin, "Noise-driven wave transitions on a vertically falling film," J. Fluid Mech. **462**, 255 (2002).
[46]C. Bielarz and S. Kalliadasis, "Time-dependent free-surface thin film flows over topography," Phys. Fluids **15**, 2512 (2003).
[47]D. D. Joseph, *Stability of Fluid Motions I* (Springer, New York, 1976).
[48]M. C. Cross and P. C. Hohenberg, "Pattern formation outside of equilibrium," Rev. Mod. Phys. **65**, 851 (1993).
[49]A. C. Newell, T. Passot, and J. Lega, "Order parameter equations for patterns," Annu. Rev. Fluid Mech. **25**, 399 (1993).
[50]P. Colinet, J. C. Legros, and M. G. Velarde, *Nonlinear Dynamics of Surface-Tension Driven Instabilities* (Wiley-VCH, Berlin, 2001).
[51]E. R. Tracy and X. Z. Tang, "Anomalous scaling behavior in Takens–Bogdanov bifurcations," Phys. Lett. A **242**, 239 (1998).
[52]S. Kalliadasis, "Nonlinear instability of a contact line driven by gravity," J. Fluid Mech. **413**, 355 (2000).
[53]S. M. Troian, E. Herbolzehimer, S. A. Safran, and J. F. Joanny, "Fingering instabilities of driven spreading films," Europhys. Lett. **10**, 25 (1989).
[54]M. A. Spaid and G. M. Homsy, "Stability of Newtonian and viscoelastic dynamic contact lines," Phys. Fluids **8**, 460 (1996).
[55]D. E. Kataoka and S. M. Troian, "A theoretical study of instabilities at the advancing front of thermally driven coating films," J. Colloid Interface Sci. **192**, 350 (1997).
[56]J. M. Davis and S. M. Troian, "Influence of attractive van der Waals interactions on the optimal excitations in thermocapillary-driven spreading," Phys. Rev. E **67**, 016308 (2003).
[57]J. M. Davis, D. E. Kataoka, and S. M. Troian, "Transient dynamics and structure of optimal excitations in thermocapillary spreading," Phys. Fluids **18**, 092101 (2006).
[58]B. F. Farrell and P. J. Ioannou, "Generalized stability theory. Part 2: Nonautonomous operators," J. Atmos. Sci. **53**, 2041 (1996).
[59]E. A. Chinnov and O. A. Kabov, "The effect of three-dimensional deformations on local heat transfer to a nonuniformly heated falling film of liquid," High Temp. **42**, 267 (2004).
[60]D. V. Zaitsev and O. A. Kabov, "Study of the thermocapillary effect on a wavy falling film using a fiber optical thickness probe," Exp. Fluids **39**, 712 (2005).
[61]J. M. Davis and S. M. Troian, "Generalized linear stability of noninertial coating flows over topographical features," Phys. Fluids **17**, 072103 (2005).
[62]S. Kalliadasis and G. M. Homsy, "Stability of free-surface thin-film flows over topography," J. Fluid Mech. **448**, 387 (2001).
[63]U. Thiele and E. Knobloch, "Driven drops on heterogeneous substrates: Onset of sliding motion," Phys. Rev. Lett. **97**, 204501 (2006).
[64]U. Thiele and E. Knobloch, "On the depinning of a driven drop on a heterogeneous substrate," New J. Phys. **8**, 313 (2006).
[65]Ph. Beltrame, P. Hanggi, and U. Thiele, "Depinning of three-dimensional drops from wettability defects," Europhys. Lett. **86**, 24006 (2009).